




Electromagnetic response in spiral magnets and emergent inductance

Daichi Kurebayashi^{1,3} & Naoto Nagaosa^{1,2}

Emergent electromagnetism in magnets originates from the strong coupling between conduction electron spins and those of noncollinear ordered moments and the consequent Berry phase. This offers possibilities to develop new functions of quantum transport and optical responses. The emergent inductance in spiral magnets is an example recently proposed and experimentally demonstrated, using the emergent electric field induced by alternating currents. However, the microscopic theory of this phenomenon is missing, which should reveal factors to determine the magnitude, sign, frequency dependence, and nonlinearity of the inductance L . Here we theoretically study electromagnetic responses of spiral magnets by taking into account their collective modes. In sharp contrast to collinear spin-density wave, the system remains metallic even in one dimension, and the canonical conjugate relation of uniform magnetization and phason coordinate plays an essential role, determining the properties of L . This result opens a way to design the emergent inductance of desired properties.

¹RIKEN Center for Emergent Matter Science (CEMS), Wako 351-0198, Japan. ²Department of Applied Physics, University of Tokyo, 7-3-1 Hongo, Bunkyo-ku, Tokyo 113-8656, Japan. ³Present address: School of Physics, The University of New South Wales, Sydney, NSW 2052, Australia.
email: d.kurebayashi@unsw.edu.au

Quantum transport phenomena in magnets include variety of effects such as magneto-resistance^{1–3}, planar Hall effect⁴, spin-dependent tunneling⁵, anomalous Hall effect^{6–10}, and spin Hall effect^{11–16}. Spin-orbit interaction is often relevant to these phenomena, because the transport reflects the orbital motion of electrons while the magnetism comes from electron spins. In addition to the conventional ferromagnetism and antiferromagnetism, recent focus is the noncollinear spin structures, which are induced by several mechanisms, e.g., frustrated exchange interaction¹⁷, Ruderman–Kittel–Kasuya–Yosida interaction^{18–24}, Fermi surface nesting^{25,26}, and Dzyaloshinskii–Moriya spin-orbit interaction^{27–29}. Note that there are situations where the system shows noncollinear spins without the spin-orbit interaction, which we study below. Noncollinear spin configurations are associated with the quantal Berry phase³⁰. The quantal Berry phase produces the emergent electromagnetic field^{31–33}; emergent electric field \mathbf{e} is defined as

$$e_i = -\frac{1}{c} \frac{\partial a_i}{\partial t} = \frac{\hbar}{2e} \mathbf{n} \cdot (\partial_i \mathbf{n} \times \partial_t \mathbf{n}), \quad (1)$$

while the emergent magnetic field \mathbf{b} by

$$b_i = (\nabla \times \mathbf{a})_i = \frac{\hbar}{2e} \varepsilon_{ijk} \mathbf{n} \cdot (\partial_j \mathbf{n} \times \partial_k \mathbf{n}), \quad (2)$$

where \mathbf{n} is the direction of the spin. Note here that \mathbf{b} is associated with the noncoplanar spin structure such as the skyrmion, while \mathbf{e} is induced by the dynamics of spins. The emergent electromagnetic field is the origin of many electromagnetic phenomena including the topological Hall effect by \mathbf{b} ^{34–37} and emergent electromagnetic induction by \mathbf{e} ³⁸.

A helical or spiral spin structure with a single wavevector \mathbf{Q} is a noncollinear but coplanar structure with $\mathbf{b} = \mathbf{0}$ in the ground state, while \mathbf{e} is induced by its dynamics. Recently, it has been proposed that the alternating current driven motion of the spiral leads to the inductance L , which is inversely proportional to the cross-section A of the sample in sharp contrast to the conventional inductor with L being proportional to A ^{39,40}. The mechanism is based on the spin-transfer torque; the angular momentum transfer between the conduction electrons and magnetic structure drives the motion of the latter, which produces the emergent electric field given by Eq. (1). In this picture, the quantum dynamics of the conduction electrons is not treated on the microscopic basis and only their current density j appears in the analysis.

Experimentally, the inductance L of a short-period helimagnet $\text{Gd}_3\text{Ru}_4\text{Al}_{12}$ has been observed⁴¹. The value of L is around ~ 100 nH, which is comparable to the best commercial value, while the size of the sample is $\sim 10^{-5}$ smaller. Here there appeared several issues. One is the sign of the inductance L . Usually, the magnetic energy induced by the current is given by $LI^2/2$ (I : current) and the negative L means that the system is unstable. Therefore, it is urgent to understand what determines the sign of L and its relation to the stability of the system. The second important issue is frequency dependence. The quality factor $Q(\omega)$ is given by $Q(\omega) = L\omega/R$ with R being the resistance and ω the angular frequency. Experimentally, the Debye-type ω -dependence with the cut-off of the order of 10kHz has been observed⁴¹. This limits the value of $Q(\omega)$, and a wider range of frequency is needed for the applications. The third one is the nonlinearity with respect to the current density. The tilt angle ϕ is expanded in the current density j as $\phi = Aj + Bj^3 + Cj^5$, and this phenomenological expression well describes the experimental result⁴¹. However, the microscopic understanding of this nonlinearity is missing. Recently, Ieda and Yamane⁴⁰ studied a related problem taking into account the Rashba spin-orbit interaction together with the

nonadiabatic β -term. They found the sign change of L from positive to a negative value as β increases.

In this paper, we microscopically derive an emergent inductance in spiral magnets by the linear response theory and determine the role of collective magnetic excitations in the emergent induction. Furthermore, by introducing nonlinear pinning potentials, we discuss the nonlinearity in the emergent inductance and the effect of the depinning transition of the magnetic excitations to the sign of the inductance.

Results

Models. In this paper, we study the microscopic model of a spiral magnet composed of one-dimensional electrons coupled with localized spins by exchange interaction. The spiral order occurs at $Q = 2k_F$ with k_F being the Fermi wavenumber of the conduction electrons. This can be regarded as the Ruderman–Kittel–Kasuya–Yosida interaction^{25,26} or the Peierls instability^{42,43}. Assuming that Q is incommensurate with the original lattice, the spiral order breaks two kinds of symmetries, i.e., the translational symmetry and the SU(2) spin rotational symmetry. The resulting symmetry is the combination of these two, i.e., the translation combined with the spin rotation, and hence the number of the Goldstone boson is 3 in the absence of the spin-orbit interaction. Two of which are the fluctuation of the plane of the spin rotation, and the last one is the so-called phason corresponding to ψ in the expression of the director \mathbf{n} of the localized spin which acts as the order parameter;

$$\mathbf{n}(\mathbf{r}) = \eta_1 \cos(\mathbf{Q} \cdot \mathbf{r} + \psi) + \eta_2 \sin(\mathbf{Q} \cdot \mathbf{r} + \psi) + \eta_3 \mathbf{m}, \quad (3)$$

where η_i is a unit vector in a Cartesian coordinates. Here note that the uniform spin component m perpendicular to the spin rotating plane is the generator of ψ corresponding to the “momentum” of the “coordinate” ψ . The basic idea of the present paper is that the inductance L of the system is related to the imaginary part of the complex impedance $Z(\omega)$, which is inverse of the conductance $\Sigma(\omega)$. Both the spin-transfer torque and the resultant emergent electric field are included in the conductance $\Sigma(\omega)$ due to the collective modes of the spiral spins, i.e., the uniform magnetization and phason. Here some remarks are in order about the difference between the spiral magnet and the conventional collinear spin density wave, which share a similar phason collective mode. One is that the system remains metallic even in the perfectly nested case for the spiral state while it is gapped in the collinear spin density wave. In the latter case, the broken symmetry is the translational symmetry and the spin rotational symmetry. The Goldstone mode corresponding to the former is the phason, while that for the latter is the spin-wave. These two are decoupled in the bilinear order, and only the phason contributes to the conductivity. The phason is usually pinned by the impurity, showing the finite pinning frequency of its spectrum. In sharp contrast, the phason in spiral magnet remains gapless even with the disorder as long as the spin rotational symmetry of the Hamiltonian is intact. Both the impurity/commensurability and the spin-orbit are needed to gap the phason spectrum there.

As a microscopic model of electrons coupled to a spiral spin order, we have considered

$$H = \int \frac{dk}{2\pi} \left[\mathbf{c}_k^\dagger \left(\frac{k^2}{2m_e} - E_F - Jm_z(t)\sigma_z \right) \mathbf{c}_k - eA(t)\mathbf{c}_k^\dagger v_k \mathbf{c}_k - J \left(\mathbf{m}_Q(t) \cdot \mathbf{c}_{k+\frac{Q}{2}}^\dagger \sigma \mathbf{c}_{k-\frac{Q}{2}} + \mathbf{m}_Q^*(t) \cdot \mathbf{c}_{k-\frac{Q}{2}}^\dagger \sigma \mathbf{c}_{k+\frac{Q}{2}} \right) \right], \quad (4)$$

where \mathbf{c}_k is a Fermion annihilation operator with momentum k , $E_F = \frac{Q^2}{8m_e}$ is the Fermi energy, m_e is an effective electron mass, J is

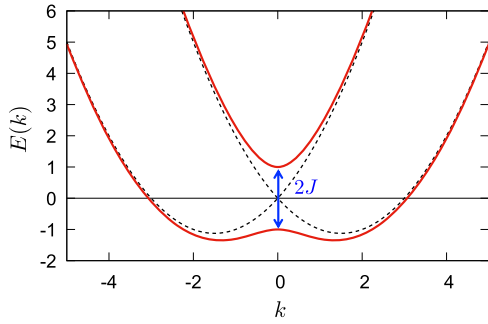


Fig. 1 Band dispersion of one-dimensional spiral magnets. The electron mass is $m_e = 1$, the exchange coupling constant is $J = 1$, and the amplitude of the propagation vector is $Q = 3$.

an exchange constant, σ is the Pauli matrix vector corresponding electron's spin operators, v_k is a group velocity operator, $A(t)$ is an electromagnetic vector potential, $\mathbf{m}_Q(t) = \frac{\hat{x} + i\hat{y}}{2} e^{-i\psi(t)} \approx \frac{\hat{x} + i\hat{y}}{2} [1 - i\psi(t)]$ characterizes the spiral magnetic order whose wave vector is magnitude of $Q = 2k_F$ and a spin rotation plane is $s_x - s_y$ plane, $\psi(t)$ is a dynamical phase degrees of freedom, namely phason, and $m_z(t)$ is a uniform moment. Note that we have considered one-dimensional free electrons just for simplicity; however, our analysis is general and applicable for higher dimensions (please see the Supplementary Note 1 for the detail) and systems with spin-orbit coupling. By introducing the spinor, $\Psi_k = [c_{k+\frac{Q}{2}, \uparrow}, c_{k-\frac{Q}{2}, \downarrow}]^T$, the Hamiltonian is simplified as

$$H = \int \frac{dk}{2\pi} \Psi_k^\dagger \left[\hat{h}_0(k) + \hat{j}_k A(t) + \hat{S}_\psi \psi(t) + \hat{S}_z m_z(t) \right] \Psi_k \quad (5)$$

where $\hat{h}_0(k) = \frac{k^2}{2m_e} \tau_0 + \frac{Qk}{2m_e} \tau_z - J\tau_x$ is the unperturbed mean field Hamiltonian, $\hat{j}_k = -e \left(\frac{k}{m_e} \tau_0 + \frac{Q}{2m_e} \tau_z \right)$ is a current operator, $\hat{S}_\psi = J\tau_y$ and $\hat{S}_z = -J\tau_z$ are spin operators coupled to phason and uniform magnetization, respectively, and τ is a vector of the Pauli matrix. The eigenvalues of $\hat{h}_0(k)$ are given by $\xi_{k,\pm} = \frac{k^2}{2m_e} \pm \sqrt{\left(\frac{Qk}{2m_e}\right)^2 + J^2}$. The band structure is shown in Fig. 1. As mentioned, the dispersion retains the metallic Fermi surfaces in addition to the gap of $\Delta = 2J$ at $k=0$ due to the nesting of the Fermi surface. With a basis diagonalizing the mean field Hamiltonian $\hat{h}_0(k)$, the current and the spin operators are expressed as

$$\tilde{j}_k = -\frac{e}{m_e} \begin{bmatrix} k - \frac{Q^2 k}{4m_e \zeta} & -\frac{iQ}{2\zeta} \\ -\frac{iQ}{2\zeta} & k + \frac{Q^2 k}{4m_e \zeta} \end{bmatrix}, \quad \tilde{S}_z = \frac{J}{\zeta} \begin{bmatrix} \frac{Qk}{2m_e} & J \\ J & -\frac{Qk}{2m_e} \end{bmatrix}, \quad \tilde{S}_\psi = J \begin{bmatrix} 0 & -i \\ i & 0 \end{bmatrix}, \quad (6)$$

where $\zeta \equiv \sqrt{\left(\frac{Qk}{2m_e}\right)^2 + J^2}$.

As a model describing the magnetic excitations, we consider the following Lagrangian for the uniform moment and the phason,

$$L_M = -m_z(t) \dot{\psi}(t) - \frac{K_z}{2} m_z^2(t) - \frac{K_\psi}{2} \psi^2(t) - l_a \langle S_z \rangle(t) m_z(t) - l_a \langle S_\psi \rangle(t) \psi(t), \quad (7)$$

where the first term is the Berry phase term representing the canonical conjugate relation between the phason $\psi(t)$ and the uniform magnetization $m_z(t)$, the second and the third terms are mass terms of excitations with a gap size of K_ψ and K_z , and l_a is a lattice constant. Each excitation gap, K_z and K_ψ , corresponds to the

intrinsic and the extrinsic pinning frequency of the spiral, respectively. Note that the excitation gap of phason K_ψ is originally zero as the phason is a Goldstone mode associated with the spontaneous breaking of translational and spin rotation symmetries. Therefore, the excitation gap of phason becomes finite when magnetic impurities or nonmagnetic impurities with spin-orbit interaction are present. The last two terms describe coupling to itinerant electron's spin density. In addition, the Rayleigh dissipation function, $R_d = \frac{\alpha}{2} [\dot{m}_z^2(t) + \dot{\psi}^2(t)]$, introduces the dissipation to magnetic excitations where α is the Gilbert damping constant.

Emergent inductance and its ω -dependence. The physical process is described by the Feynman diagram in Fig. 2^{44,45}. The right bubble corresponds to the spin accumulation induced by the external electric fields, including the spin-transfer torque effect. The left bubble corresponds to the emergent electric field, i.e., the collective modes affect the motion of the conduction electrons. The combination of these two processes contributes to the conductivity of the total system, and below, we discuss each of them separately. See Eq. (23) below. Within the linear response theory, a current density induced by magnetic excitations are given as

$$\langle j \rangle(\Omega) = \sigma_{m_z}(\Omega) m_z(\Omega) + \sigma_\psi(\Omega) \psi(\Omega), \quad (8)$$

where Ω is an external frequency, and $\sigma_{m_z}(\Omega)$ and $\sigma_\psi(\Omega)$ are conductivities related to ferromagnetic and phason excitations, respectively. Each conductivity is evaluated as

$$\begin{aligned} \sigma_{m_z}(\Omega) &= -\frac{1}{2\pi\beta} \int dk \sum_{\omega_n} \text{Tr} [\tilde{j}_k \hat{G}_k(\omega_n + \Omega_m) \hat{S}_z \hat{G}_k(\omega_n)] \Big|_{i\Omega_m \rightarrow \Omega + i0} \\ &\approx -\frac{i\tau_e \Omega}{2\pi} \sum_{i=\pm} \int dk (\tilde{j}_k)_{ii} (\tilde{S}_z)_{ii} f'(\xi_{k,i}) = -i\Omega C_{m_z}(Q), \end{aligned} \quad (9)$$

$$\begin{aligned} \sigma_\psi(\Omega) &= -\frac{1}{2\pi\beta} \int dk \sum_{\omega_n} \text{Tr} [\tilde{j}_k \hat{G}_k(\omega_n + \Omega_m) \tilde{S}_\psi \hat{G}_k(\omega_n)] \Big|_{i\Omega_m \rightarrow \Omega + i0} \\ &\approx \Omega \sum_{i \neq j} \int \frac{dk}{2\pi} \frac{(\tilde{j}_k)_{ij} (\tilde{S}_\psi)_{ji} - (\tilde{S}_\psi)_{ij} (\tilde{j}_k)_{ji}}{(\xi_{k,i} - \xi_{k,j})^2} f(\xi_{k,i}) = -i\Omega C_\psi(Q), \end{aligned} \quad (10)$$

where $\hat{G}_k(\omega_n) = [i\omega_n - \hat{h}_0(k)]^{-1}$ is a bare Green's function of \hat{h}_0 , τ_e is a scattering lifetime, $f(x)$ is the Fermi-Dirac distribution function, and $C_{m_z}(Q)$ and $C_\psi(Q)$ are coefficients characterizing uniform moment and phason conductivities, respectively. The analytical expressions of the coefficients are given by $C_{m_z}(Q) = \frac{eQ\tau_e}{4\pi\zeta\sqrt{m_e}} \sqrt{\zeta' - \frac{Q^2}{2m_e} \left(\zeta' + \frac{Q^2}{2m_e} \right)}$ and $C_\psi(Q) = \frac{eQ}{2\pi\sqrt{m_e} \sqrt{\zeta' + \frac{Q^2}{2m_e}}}$ where

$\zeta' = \sqrt{\left(\frac{Q^2}{2m_e}\right)^2 + 4J^2}$. When $\frac{Q^2}{2m_e} \ll 2|J|$ corresponding to long pitch spirals or the adiabatic limit, the coefficients are simplified as $C_{m_z} = \frac{eQ\tau_e J}{\pi\sqrt{8}m_e}$ and $C_\psi = \frac{eQ}{\pi\sqrt{8}m_e}$, which is linear in Q . On the other hand, for short pitch spirals or the nonadiabatic limit where $\frac{Q^2}{2m_e} \gg 2|J|$ is satisfied, the coefficients are given as $C_{m_z} = \frac{e\tau_e J}{\pi}$ and $C_\psi = \frac{e}{2\pi}$, which is independent of Q . Note, however, that our analysis is basically the random phase approximation, which is justified in the weak coupling limit, i.e., $\frac{Q^2}{2m_e} \gg 2|J|$. Also, since our primary interests are in the nonadiabatic limits, we focus on $Q \rightarrow \infty$ limits in the rest of the manuscript. In Eqs. (9) and (10), we have performed the analytical continuation, $i\Omega_m \rightarrow \Omega + i0$.

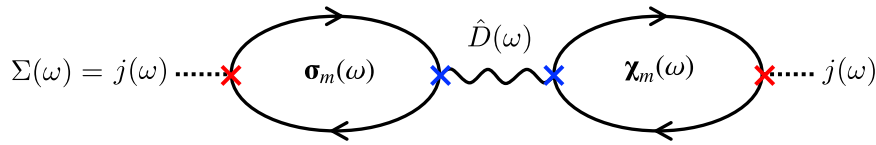


Fig. 2 The Feynman diagram describing the conductivity mediated by magnetic excitations, $\Sigma(\omega)$. The left electron bubble corresponds to the conductivity induced by the magnetic excitations, σ_m , while the right electron bubble is the electromagnetic susceptibility, χ_m . The solid (wave) line is propagators of itinerant electrons (magnetic excitations $\hat{D}(\omega)$).

We have also expanded the response functions with respect to the external frequency Ω up to the first order; however, the zeroth-order in Ω vanishes. Because \tilde{j}_k and \tilde{S}_z are symmetric matrices, the conductivity related to ferromagnetic excitation, σ_{m_z} , is given by diagonal elements of $(\tilde{j}_k)_{ij}(\tilde{S}_z)_{ji}$; only states near the Fermi surface contribute to σ_{m_z} . Contrary, the phason spin operator \tilde{S}_ψ only consists of off-diagonal elements; namely, only inter-band transitions contribute to the phason conductivity. This difference is reflected in the lifetime dependence of the conductivities; σ_{m_z} is proportional to the lifetime τ_e which is a typical characteristic of the Fermi surface contribution, whereas σ_ψ is independent of τ_e , indicating that the phason contribution originates from all occupied states. Let us note that the vertex correction does not give the leading order contribution to the conductivities in the clean limit, $\tau_e \rightarrow \infty$. For more details on the effect of the vertex correction, please see the Supplementary Note 2. Finally, the current density induced by magnetic excitations is summarized as

$$\langle j \rangle(\Omega) = -i\Omega C_{m_z} m_z(\Omega) - i\Omega C_\psi \psi(\Omega) = -i\Omega \frac{eJ\tau_e}{\pi} m_z(\Omega) - i\Omega \frac{e}{2\pi} \psi(\Omega). \quad (11)$$

Then, let us consider the spin densities induced by applied electric fields,

$$\langle S_\psi \rangle(\Omega) = \chi_\psi(\Omega) A(\Omega), \quad (12)$$

$$\langle S_z \rangle(\Omega) = \chi_{m_z}(\Omega) A(\Omega), \quad (13)$$

where χ_{m_z} and χ_ψ are electromagnetic susceptibilities, and $\langle S_\psi \rangle$ and $\langle S_z \rangle$ are spin densities coupled to phason and uniform magnetization, respectively. The susceptibilities are evaluated as

$$\chi_\psi(\Omega) = -\frac{1}{2\pi\beta} \int dk \sum_{\omega_n} \text{Tr} \left[\hat{S}_\psi \hat{G}_k(\omega_n + \Omega_m) \hat{j}_k \hat{G}_k(\omega_n) \right] = -\sigma_\psi(\Omega), \quad (14)$$

$$\chi_{m_z}(\Omega) = -\frac{1}{2\pi\beta} \int dk \sum_{\omega_n} \text{Tr} \left[\hat{S}_z \hat{G}_k(\omega_n + \Omega_m) \hat{j}_k \hat{G}_k(\omega_n) \right] = \sigma_{m_z}(\Omega). \quad (15)$$

Similar to the relation between the spin-transfer torque and the spin motive force⁴⁶, the spin densities induced by applied electric fields are related to the current response driven by magnetic excitations. It is worth mentioning that the phason contribution has an opposite sign with conductivity, whereas the contribution from uniform magnetization has the same sign. The difference attributes to the fact that the phason response comes from an inter-band contribution while the uniform moment excitation comes from the intra-band contribution. In other words, the uniform moment contribution, $C_{m_z}(Q)$, is a transport-like contribution, and the phason contribution, $C_\psi(Q)$, is a geometric contribution. Finally, the spin densities induced by an applied electric field is obtained as

$$\langle S_\psi \rangle(\Omega) = i\Omega C_\psi A(\Omega) = -\frac{e}{2\pi} E(\Omega), \quad (16)$$

$$\langle S_z \rangle(\Omega) = -i\Omega C_{m_z} A(\Omega) = \frac{eJ\tau_e}{\pi} E(\Omega), \quad (17)$$

where $E(\Omega) = -i\Omega A(\Omega)$ is the applied electric field.

As current and magnetic responses in itinerant electrons have been evaluated, the magnetic dynamics under an applied electric field are considered in the following. Applying the Euler-Lagrange equation, $\frac{\delta L_M}{\delta q} - \frac{d}{dt} \frac{\delta L_M}{\delta \dot{q}} - \frac{\delta R_d}{\delta q} = 0$, to the Lagrangian, Eq. (7), and the Rayleigh dissipation function, we obtain the equations of motions for m_z and ψ as

$$\dot{m}_z(t) - K_\psi \psi(t) - \alpha \dot{\psi}(t) - l_a \langle S_\psi \rangle(t) = 0, \quad (18)$$

$$-\dot{\psi}(t) - K_z m_z(t) - \alpha \dot{m}_z(t) - l_a \langle S_z \rangle(t) = 0. \quad (19)$$

A solution of the equations are obtained as

$$\begin{bmatrix} \psi(\omega) \\ m_z(\omega) \end{bmatrix} = l_a \hat{D}(\omega) \begin{bmatrix} \langle S_\psi \rangle(\omega) \\ \langle S_z \rangle(\omega) \end{bmatrix}, \quad (20)$$

$$\hat{D}(\omega) = \begin{bmatrix} -K_\psi + i\alpha\omega & -i\omega \\ i\omega & -K_z + i\alpha\omega \end{bmatrix}^{-1}, \quad (21)$$

where we have shifted to a frequency representation and $\hat{D}(\omega)$ is a Green's function for magnetic excitations.

By equating Eqs. (11), (16), (17), and (20), the current density is evaluated as $\langle j \rangle(\omega) = \Sigma(\omega) E(\omega)$ where a complex conductivity is given by

$$\Sigma(\omega) = \sigma_m^T(\omega) \hat{D}(\omega) \chi_m(\omega) / l_a \quad (22)$$

where $\sigma_m = [\sigma_\psi, \sigma_{m_z}]^T$ and $\chi_m = [\chi_\psi, \chi_{m_z}]^T$. Here, we have converted the one-dimensional current density to the three-dimensional current by $\langle j_{3D} \rangle = \langle j_{1D} \rangle / l_a^2$. The impedance $Z(\omega)$ is determined as an inverse of the complex conductivity, $Z(\omega) = \frac{l_a}{A} [\sigma_{dc} + \Sigma(\omega)]^{-1}$ where $\sigma_{dc} = \frac{e^2 Q \tau_e}{2\pi m_e l_a^2}$ is the DC conductivity which is irrelevant to the magnetic excitations, A is a cross section of the system, and l_s is a length between electrodes. Then the complex inductance is defined as $L(\omega) = Z(\omega) / (-i\omega)$. In the absence of impurity pinning where the phason excitation is gapless, $K_\psi = 0$, a real part of the inductance, as shown in Fig. 3a, takes positive value when $\omega < \omega_{int}$ where $\omega_{int} = \alpha K_z$ is an intrinsic pinning frequency corresponding to the excitation of uniform moments, while rapidly decreases above ω_{int} . At the same time, the imaginary part of the inductance peaks at ω_{int} , showing the characteristic behavior of the Debye-type relaxation. In contrast, when impurity pinning are present, an additional peak structure at $\omega = \omega_{ext}$ where $\omega_{ext} \sim \sqrt{K_\psi K_z}$ associated with the phason excitation appears on the imaginary part of inductance as shown in Fig. 3b. The real part of the inductance is negative with the typical parameters when $\omega < \omega_{ext}$ while showing the sign change above ω_{ext} .

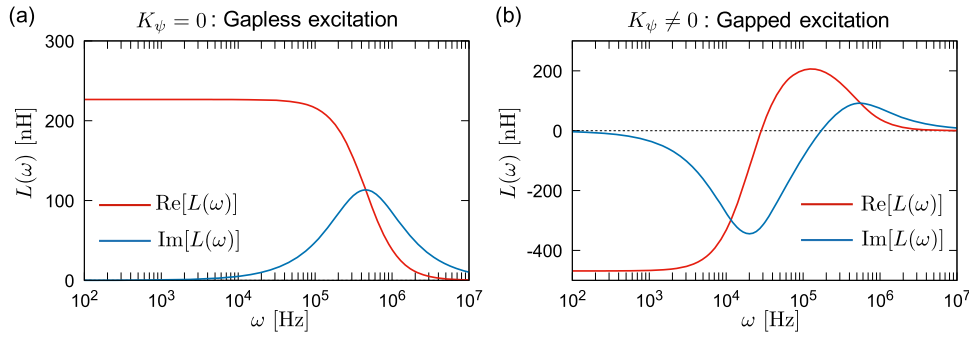


Fig. 3 Frequency dependence of the emergent inductance $L(\omega)$. **a** The inductance for the gapless phason ($K_\psi = 0$) is plotted as a function of frequency ω . **b** The inductance for the gapped phason ($K_\psi = 10^4$ Hz) is plotted as a function of frequency ω . The red (blue) line shows the real- (imaginary-) part of the inductance. Other parameters are the pinning potential for the uniform moment $K_z = 10^6$ Hz, the exchange coupling constant $J = 200$ meV, the scattering lifetime of electrons $\tau_e = 10$ fs, the cross section of the system $A = 10 \mu\text{m}^2$, the lattice constant $l_a = 4 \text{ \AA}$, the distance between electrodes $l_s = 10 \mu\text{m}$, the Gilbert damping constant $\alpha = 0.5$, and the propagation vector of spiral $Q = 2.24 \text{ nm}^{-1}$.

In the low-frequency limit, the impedance can be expanded as $Z(\omega) \approx \frac{l_s}{\sigma_{\text{dc}} + \text{Re}[\Sigma(\omega)]} - i\omega l_s \frac{\text{Im}[\Sigma(\omega)/\omega]}{(\sigma_{\text{dc}} + \text{Re}[\Sigma(\omega)])^2}$. Comparing with the conventional expression, $Z(\omega) = R - i\omega L$, where R is a resistance and L is an inductance, one can regard the imaginary part of the complex conductivity as the inductance of spiral;

$$L = l_s \frac{\text{Im}[\Sigma(\omega)/\omega]}{(\sigma_{\text{dc}} + \text{Re}[\Sigma(\omega)])^2} \Big|_{\omega \rightarrow 0}. \quad (23)$$

Note that the equivalence of the imaginary part of the conductivity and the inductance is valid when the real part of the conductivity is larger than its imaginary part, namely $\sigma_{\text{dc}} + \text{Re}[\Sigma(\omega)] \gg \text{Im}[\Sigma(\omega)]$.

In the following, we will discuss what determines the sign of the inductance. Let us first consider the case for the gapless phason excitation. The complex conductivity $\Sigma(\omega)$ and the inductance L for the gapless phason are obtained as

$$\Sigma(\omega) = \frac{C_\psi^2}{l_a \alpha} + i\omega \frac{(C_\psi + \alpha C_{m_z})^2}{l_a \alpha^2 K_z} = \frac{e^2}{4\pi^2 l_a \alpha} + i\omega \frac{e^2 (1 + 2\alpha\tau_e J)^2}{4\pi^2 l_a \alpha^2 K_z}, \quad (24)$$

$$L = \frac{l_s e^2}{4\pi^2 l_a A (\sigma_{\text{dc}} + \frac{e^2}{4\pi^2 l_a \alpha})^2} \frac{(1 + 2\alpha\tau_e J)^2}{\alpha^2 K_z}. \quad (25)$$

The expression suggests that both the real and imaginary parts of the complex conductivity is always positive. As a result, the sign of the inductance is also positive when the phason excitation is gapless. On the other hand, in the gapped phason regime, the conductivity and the inductance mediated by magnetic excitations are obtained as

$$\Sigma(\omega) = \frac{i\omega}{l_a} \left(\frac{C_{m_z}^2}{K_z} - \frac{C_\psi^2}{K_\psi} \right) = \frac{i\omega e^2}{l_a 4\pi^2} \left(\frac{4\tau_e^2 J^2}{K_z} - \frac{1}{K_\psi} \right), \quad (26)$$

$$L = \frac{l_s e^2}{4\pi^2 l_a A \sigma_{\text{dc}}^2} \left(\frac{4\tau_e^2 J^2}{K_z} - \frac{1}{K_\psi} \right). \quad (27)$$

The result shows that the imaginary part of the conductivity can take both the positive and negative signs when the magnetic excitation is gapped. Equation (26) consists of two terms; the first term is described by the response function and the characteristic frequency of uniform moment excitations, while those of phason excitation give the second term. Although m_z and ψ are not independent excitations, the result can be seen as the uniform moment and phason contributions compete to determine the

overall sign of the inductance. Let us refer to these two contributions to a m_z -contribution and a ψ -contribution in the rest of the manuscript. The result in Eq. (27) has some similarity to the result previously reported⁴⁰, although an approach is different; their analysis is based on spin-transfer torques and spin motive force while we have evaluated the complex conductivity based on a microscopic linear response theory. Note that the negative inductance does not correspond to the instability of the system as it is not related to the magnetic energy. Instead, in our approach evaluating the current-current correlation, the negative inductance means that the imaginary part of the complex conductivity is negative. A detailed discussion on the stability of the system is presented in ‘‘Discussion’’ section.

Depinning transition and nonlinear effects. Now we consider the effect of the depinning of phason on the conductance. It is known that there is a threshold field strength⁴⁷ to drive magnetic spirals. The dynamics of the texture is confined around pinning centers under the threshold field; the inductance for the pinned magnetic spiral, Eq. (27), is expected. On the other hand, above the threshold field strength, the phason starts freely moving, and pinning potential becomes negligible. In this strong field regime, the inductance for gapless phason, Eq. (25), is expected. By substituting the magnetic potentials in Eq. (7) with periodic potentials as $\frac{K_z}{2} m_z^2 \rightarrow \frac{K_z}{4} (1 - \cos 2m_z)$ and $\frac{K_\psi}{2} \rightarrow K_\psi (1 - \cos \psi)$. The substitutions introduce the finite potential depth so that the depinning transition can be discussed. We have numerically solved the equations of motion, Eqs. (18) and (19), with the nonlinear potentials and perform the Fourier transformation to obtain $\psi(\omega)$ and $m_z(\omega)$, then evaluated current density by Eq. (11). The applied electric field amplitude (E_0) dependence of the emergent inductance is shown in Fig. 4a. In the weak-field regime, the sign of the inductance is negative as shown in Fig. 4 corresponding to pinned magnetic excitations. By increasing the field strength, the emergent inductance decreases quadratically to the field strength; $L = c_0 + c_2 E_0^2$ where c_0 and c_2 are coefficients. Within the weak-field regime, the dynamics of the phason is confined in a potential valley around $\psi = 0$. Further increasing the field strength, the inductance shows a discontinuous jump and changes its sign, corresponding to the depinning transition. Just above the thresholds, the phason dynamics covers two valleys under the oscillating field. Multiple discontinuities in the higher field follow a change in the number of valleys that the phason moves across. Above the thresholds, the inductance shows several sign changes due to nonlinearity in the potentials. The frequency and field dependence of the emergent inductance is shown in Fig. 4b. With typical material parameters,

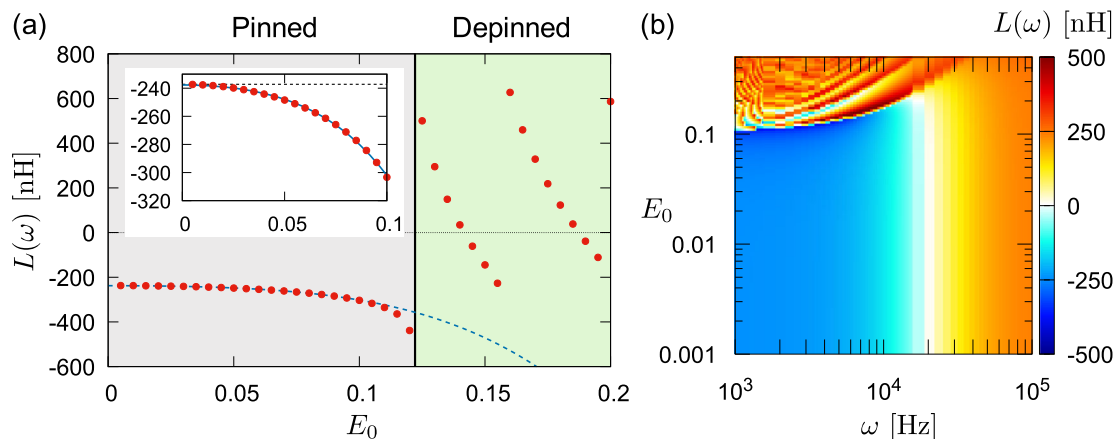


Fig. 4 The emergent inductance with nonlinear pinning potentials. **a** The emergent inductance $L(\omega)$ at $\omega = 3$ kHz is plotted as a function of the applied electric field E_0 . The inset shows the magnified behavior at the low field region. The red (blue) line shows the inductance with the phason gap $K_\psi = 10^4$ Hz (10^7 Hz). **b** The emergent inductance is plotted as a function of frequency ω and the applied field E_0 . Other parameters are the pinning potential for the uniform moment $K_z = 10^6$ Hz, the exchange coupling constant $J = 200$ meV, the scattering lifetime of electrons $\tau_e = 10$ fs, the cross section of the system $A = 10 \mu\text{m}^2$, the lattice constant $l_a = 4 \text{ \AA}$, the distance between electrodes $l_s = 10 \mu\text{m}$, the Gilbert damping constant $\alpha = 0.5$, and the propagation vector of spiral $Q = 2.24 \text{ nm}^{-1}$.

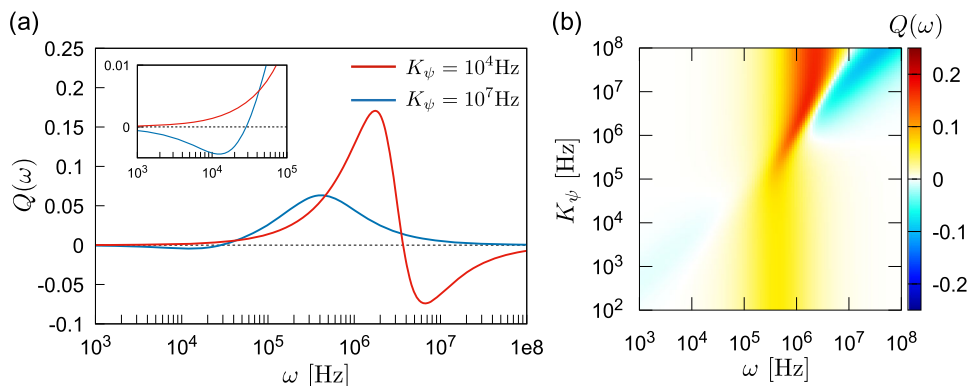


Fig. 5 The quality factor of the emergent inductance. **a** The quality factor with the phason gap $K_\psi = 10^4$ Hz and 10^7 Hz is plotted as a function of the frequency ω . The inset shows a magnified behavior at the low-frequency regime. **b** The quality factor is plotted as a function of the frequency ω and the phason excitation gap K_ψ . Other parameters are the pinning potential for the uniform moment $K_z = 10^6$ Hz, the exchange coupling constant $J = 200$ meV, the scattering lifetime of electrons $\tau_e = 10$ fs, the cross section of the system $A = 10 \mu\text{m}^2$, the lattice constant $l_a = 4 \text{ \AA}$, the distance between electrodes $l_s = 10 \mu\text{m}$, the Gilbert damping constant $\alpha = 0.5$, and the propagation vector of spiral $Q = 2.24 \text{ nm}^{-1}$.

the threshold field strength is roughly $E_c \sim 0.1 \text{ V/m}$, although the threshold field increases as frequency. Although there are oscillations attributing to nonlinearity in potentials, the emergent inductance is generally positive above E_c . These results suggest that the sign of the emergent inductance can be controlled by the external electric field. As suggested in Eq. (27), the sign of the inductance is determined by the competition between two contributions; however, these contributions are material dependent. Utilizing the nonlinearity provides an additional means to manipulate the sign of the inductance.

Quality factor: $Q(\omega)$. Finally, let us discuss the quality factor. The quality factor $Q(\omega)$ which is often used to evaluate the performance of an inductance, is defined by the ratio of the imaginary part and the real part of a complex impedance, $Q(\omega) = -\text{Im}[Z(\omega)]/\text{Re}[Z(\omega)] \approx \omega L/R$. The frequency dependence of the quality factor is presented in Fig. 5a, showing the sign change in $Q(\omega)$ at the characteristic frequency of magnetic excitations. When the extrinsic pinning frequency is smaller than the intrinsic pinning, $\omega_{\text{ext}} < \omega_{\text{int}}$, the quality factor is negative below the extrinsic pinning frequency while changes to positive above it. On the other hand, when the extrinsic pinning frequency exceeds the

intrinsic pinning frequency, the quality factor takes a positive value associated with the extrinsic pinning, then changes to negative. The frequency and the extrinsic pinning frequency dependence of the quality factor is depicted in Fig. 5b, showing that the quality factor becomes larger when $\omega_{\text{ext}} > \omega_{\text{int}}$. This suggests that the quality factor is improved by intentionally introducing impurities to increase the extrinsic pinning frequency. The quality factor is usually the order of $Q \sim 10^{-1}$ with the typical parameters in spiral magnets, whereas current commercial inductors have the order of magnitude larger quality factor, $Q = 10^1 \sim 10^2$. However, as it is inversely proportional to the resistance, a higher quality factor is expected for metals with higher mobility.

Discussion

Experimentally, negative inductance has been observed in a short-period helimagnet $Gd_3Ru_4Al_{12}$. Our result given in Eq. (27) suggests that magnetic excitations in $Gd_3Ru_4Al_{12}$ are gapped, and the phason contribution is considered to be dominant comparing to contributions from uniform moments. The Debye-type relaxation behavior shown in Fig. 3 is also observed in $Gd_3Ru_4Al_{12}$. Regarding the nonlinearity, our result given in Fig. 4

shows quadratic dependence to an applied field, $L = c_0 + c_2 E_0^2$; the same behavior was experimentally reported⁴¹. Recently, another short-pitch metallic helimagnet $Y\text{Mn}_6\text{Sn}_6$ is reported to show considerably large emergent inductance above the room temperature⁴⁸. In this compound, the inductance changes negative to positive as increasing temperature towards the phase transition temperature to the forced-ferromagnetic states. This behavior can be explained by the softening of the phason modes; in the low-temperature regime, the phason is pinned by impurities, whereas the phason is thermally excited and depinned in the high temperature near the transition. The sign change of the inductance from negative to positive by increasing applied current density is also reported. Our result shown in Fig. 4 suggests that the sign change is attributed to the depinning transition of the phason.

Let us discuss the Q -dependence of the inductance. In the previous studies based on the adiabatic approach: the spin-transfer torque and the emergent electromagnetic field^{39,40}, the inductance is predicted to be proportional to Q . Contrary, our results shown in Eqs. (25) and (27) are independent of Q when $\frac{Q^2}{2m_c} \gg 2J$. This discrepancy arises from differences in considered limits; the previous studies focus on the long pitch spiral or the adiabatic limit, whereas our focus is on the short pitch spiral or the nonadiabatic limit. Thus, our study and the previous studies are complementary. These results suggest that there is a crossover around $\frac{Q^2}{2m_c} \sim 2J$ between the adiabatic and nonadiabatic transport, and the inductance saturates and becomes independent of the pitch of the spiral as Q increases.

Lastly, we discuss the stability of the system. The negative L does not mean the negative energy for the magnetic field in the present case. Instead, it is related to the electric field with momentum $q = 0$. The stability of the system is ensured by the analyticity of conductance or conductivity in the upper half of the complex frequency plane, i.e., the causality condition is satisfied. For example, in classical electromagnetism, a resistor-inductor circuit (RL circuit) with negative inductance is known to be unstable as its transient solution is given by $I(t) \propto e^{-Rt/L}$ where $I(t)$ is a current. The conductance in this system is given by $G(\omega) = 1/(R - i\omega L)$ whose pole is located at $\omega_p = -iR/L$. When both R and L are positive, the conductance is analytical in the upper half of the complex plane, ensuring stability, whereas when the $L < 0$, the conductance is no longer analytical, and the system becomes unstable. To apply the same argument to spiral magnets, the pole of the complex conductivity, Eq. (22), are found at

$$\omega_p = \begin{cases} \pm \frac{\sqrt{4K_z K_\psi - \alpha^2 (K_z - K_\psi)^2}}{2(1+\alpha^2)} - i \frac{\alpha(K_z + K_\psi)}{2(1+\alpha^2)} & \left(\frac{\alpha^2}{4} < \frac{K_z K_\psi}{(K_z - K_\psi)^2} \right) \\ -i \frac{\sqrt{\alpha^2 (K_z - K_\psi)^2 - 4K_z K_\psi} \pm \alpha(K_z + K_\psi)}{2(1+\alpha^2)} & \left(\frac{\alpha^2}{4} > \frac{K_z K_\psi}{(K_z - K_\psi)^2} \right), \end{cases} \quad (28)$$

where all the poles are located in the lower half of the complex plane ensuring analyticity of the conductivity in the upper half of complex plane. Namely, the stability of the system is retained even with a negative inductance in spiral magnets.

In conclusion, we have microscopically derived the analytical expressions of an emergent inductance in spiral magnets based on the linear response theory of conductivity and identified the role of the phason collective modes in the emergent inductance. We revealed that the sign of inductance is positive when the phason excitation is gapless in the absence of impurity pinning, while it can be both negative and positive in the presence of pinning. For the pinned case, the sign of inductance is determined by a competition between contributions from phason and uniform magnetization excitations; phason excitation

contributes to negative inductance, and uniform moment excitation contributes to positive inductance. We further investigate the nonlinearity in emergent inductance and found that the depinning transition of the magnetic spiral can cause the sign change of inductance. This nonlinearity and depinning processes provide a way to control the sign of inductance by external electric fields. Finally, we have evaluated the quality factor and its dependence on extrinsic pinning. As a result, we found that the quality factor becomes larger when the extrinsic pinning potential exceeds the intrinsic pinning potential. We believe that our results would provide the microscopic understanding and essential knowledge for devise applications of the emergent inductance.

Methods

We use the fourth-order Runge–Kutta method to solve the equations of motion with the nonlinear potentials. We examine the real-time dynamics of the magnetic excitations under the oscillating field, $E(t) = E_0 \cos(\omega t)$, and perform the Fourier transformation to extract the first-harmonic components, $\psi(\omega)$ and $m_z(\omega)$.

Data availability

All data needed to evaluate the conclusions in the paper are present in the paper. Additional data related to this paper may be requested from the author.

Received: 29 April 2021; Accepted: 12 November 2021;

Published online: 06 December 2021

References

1. Binash, G., Grünberg, P., Saurenbach, F. & Zinn, W. Enhanced magnetoresistance in layered magnetic structures with antiferromagnetic interlayer exchange. *Phys. Rev. B* **39**, 4828–4830 (1989).
2. Baibich, M. N. et al. Giant magnetoresistance of (001)Fe/(001)Cr magnetic superlattices. *Phys. Rev. Lett.* **61**, 2472–2475 (1988).
3. Prinz, G. A. Magneto-electronics. *Science* **282**, 1660–1663 (1998).
4. McGuire, T. & Potter, R. Anisotropic magnetoresistance in ferromagnetic 3D alloys. *IEEE Trans. Magn.* **11**, 1018–1038 (1975).
5. Tedrow, P. M. & Meservey, R. Spin-dependent tunneling into ferromagnetic nickel. *Phys. Rev. Lett.* **26**, 192–195 (1971).
6. Karplus, R. & Luttinger, J. M. Hall effect in ferromagnetics. *Phys. Rev.* **95**, 1154–1160 (1954).
7. Chang, M.-C. & Niu, Q. Berry phase, hyperorbits, and the Hofstadter spectrum: semiclassical dynamics in magnetic Bloch bands. *Phys. Rev. B* **53**, 7010–7023 (1996).
8. Sundaram, G. & Niu, Q. Wave-packet dynamics in slowly perturbed crystals: gradient corrections and Berry-phase effects. *Phys. Rev. B* **59**, 14915–14925 (1999).
9. Nagaosa, N., Sinova, J., Onoda, S., MacDonald, A. H. & Ong, N. P. Anomalous Hall effect. *Rev. Mod. Phys.* **82**, 1539–1592 (2010).
10. Xiao, D., Chang, M.-C. & Niu, Q. Berry phase effects on electronic properties. *Rev. Mod. Phys.* **82**, 1959–2007 (2010).
11. Hirsch, J. E. Spin Hall effect. *Phys. Rev. Lett.* **83**, 1834–1837 (1999).
12. Murakami, S., Nagaosa, N. & Zhang, S.-C. Dissipationless quantum spin current at room temperature. *Science* **301**, 1348–1351 (2003).
13. Sinova, J. et al. Universal intrinsic Spin Hall effect. *Phys. Rev. Lett.* **92**, 126603 (2004).
14. Kato, Y. K., Myers, R. C., Gossard, A. C. & Awschalom, D. D. Observation of the Spin Hall effect in semiconductors. *Science* **306**, 1910–1913 (2004).
15. Wunderlich, J., Kaestner, B., Sinova, J. & Jungwirth, T. Experimental Observation of the Spin-Hall effect in a two-dimensional spin-orbit coupled semiconductor system. *Phys. Rev. Lett.* **94**, 047204 (2005).
16. Sinova, J., Valenzuela, S. O., Wunderlich, J., Back, C. H. & Jungwirth, T. Spin Hall effects. *Rev. Mod. Phys.* **87**, 1213–1260 (2015).
17. Yuan, H. Y., Gomony, O. & Kläui, M. Skyrmions and multisublattice helical states in a frustrated chiral magnet. *Phys. Rev. B* **96**, 134415 (2017).
18. Ruderman, M. A. & Kittel, C. Indirect exchange coupling of nuclear magnetic moments by conduction electrons. *Phys. Rev.* **96**, 99–102 (1954).
19. Kasuya, T. A theory of metallic ferro- and antiferromagnetism on Zener's model. *Prog. Theor. Phys.* **16**, 45–57 (1956).
20. Yosida, K. Magnetic properties of Cu-Mn alloys. *Phys. Rev.* **106**, 893–898 (1957).
21. Ozawa, R. et al. Vortex crystals with chiral stripes in itinerant magnets. *J. Phys. Soc. Jpn.* **85**, 103703 (2016).

22. Hayami, S., Ozawa, R. & Motome, Y. Effective bilinear-biquadratic model for noncoplanar ordering in itinerant magnets. *Phys. Rev. B* **95**, 224424 (2017).
23. Bezvershenko, A. V., Kolezhuk, A. K. & Ivanov, B. A. Stabilization of magnetic skyrmions by RKKY interactions. *Phys. Rev. B* **97**, 054408 (2018).
24. Cacilhas, R. et al. Coupling of skyrmions mediated by the RKKY interaction. *Appl. Phys. Lett.* **113**, 212406 (2018).
25. Klinovaja, J., Stano, P., Yazdani, A. & Loss, D. Topological superconductivity and Majorana fermions in RKKY systems. *Phys. Rev. Lett.* **111**, 186805 (2013).
26. Kim, Y., Cheng, M., Bauer, B., Lutchyn, R. M. & Das Sarma, S. Helical order in one-dimensional magnetic atom chains and possible emergence of Majorana bound states. *Phys. Rev. B* **90**, 060401 (2014).
27. Dzyaloshinsky, I. A thermodynamic theory of “weak” ferromagnetism of antiferromagnetics. *J. Phys. Chem. Solids* **4**, 241–255 (1958).
28. Moriya, T. Anisotropic superexchange interaction and weak ferromagnetism. *Phys. Rev.* **120**, 91–98 (1960).
29. Sergienko, I. A. & Dagotto, E. Role of the Dzyaloshinskii-Moriya interaction in multiferroic perovskites. *Phys. Rev. B* **73**, 094434 (2006).
30. Berry, M. V. Quantal phase factors accompanying adiabatic changes. *Proc. R. Soc. Lond., A Math. Phys. Sci.* **392**, 45–57 (1984).
31. Volovik, G. E. Linear momentum in ferromagnets. *J. Phys. C*, **20**, L83–L87 (1987).
32. Fröhlich, J. & Studer, U. M. Gauge invariance and current algebra in nonrelativistic many-body theory. *Rev. Mod. Phys.* **65**, 733–802 (1993).
33. Nagaosa, N. & Tokura, Y. Emergent electromagnetism in solids. *Phys. Scr.* **T146**, 014020 (2012).
34. Taguchi, Y., Oohara, Y., Yoshizawa, H., Nagaosa, N. & Tokura, Y. Spin chirality, berry phase, and anomalous Hall effect in a frustrated ferromagnet. *Science* **291**, 2573–2576 (2001).
35. Machida, Y. et al. Unconventional anomalous Hall effect enhanced by a noncoplanar spin texture in the Frustrated Kondo lattice $\text{Pr}_2\text{Ir}_2\text{O}_7$. *Phys. Rev. Lett.* **98**, 057203 (2007).
36. Neubauer, A. et al. Topological Hall effect in the A phase of MnSi. *Phys. Rev. Lett.* **102**, 186602 (2009).
37. Nagaosa, N. & Tokura, Y. Topological properties and dynamics of magnetic skyrmions. *Nat. Nanotechnol.* **8**, 899–911 (2013).
38. Barnes, S. E. & Maekawa, S. Generalization of Faraday’s law to include nonconservative spin forces. *Phys. Rev. Lett.* **98**, 246601 (2007).
39. Nagaosa, N. Emergent inductor by spiral magnets. *Jpn. J. Appl. Phys.* **58**, 120909 (2019).
40. Ieda, J. & Yamane, Y. Intrinsic and extrinsic tunability of Rashba spin-orbit coupled emergent inductors. *Phys. Rev. B* **103**, L100402 (2021).
41. Yokouchi, T. et al. Emergent electromagnetic induction in a helical-spin magnet. *Nature* **586**, 232–236 (2020).
42. Grüner, G. The dynamics of charge-density waves. *Rev. Mod. Phys.* **60**, 1129–1181 (1988).
43. Grüner, G. The dynamics of spin-density waves. *Rev. Mod. Phys.* **66**, 1–24 (1994).
44. Lee, P., Rice, T. & Anderson, P. Conductivity from charge or spin density waves. *Solid State Commun.* **14**, 703–709 (1974).
45. Nakane, Y., Miyazawa, H. & Takada, S. Impurity pinning and microwave conductivity of incommensurate spin density waves. *J. Phys. Soc. Jpn.* **57**, 3424–3444 (1988).
46. Hals, K. M. D. & Brataas, A. Spin-motive forces and current-induced torques in ferromagnets. *Phys. Rev. B* **91**, 214401 (2015).
47. Tataru, G., Kohno, H. & Shibata, J. Microscopic approach to current-driven domain wall dynamics. *Phys. Rep.* **468**, 213–301 (2008).
48. Kitaori, A. et al. Emergent electromagnetic induction beyond room temperature. *Proc. Natl Acad. Sci. U.S.A.* **118**, e2105422118 (2021).

Acknowledgements

The authors are grateful to J. Ieda, Y. Yamane, K. Yamamoto, S. Maekawa, Y. Tokura, M. Hirschberger, A. Kitaori, and Y. Yokouchi for insightful discussions. D.K. was supported by the RIKEN Special Postdoctoral Researcher Program. N.N. was supported by JST CREST Grant Number JPMJCR1874 and JPMJCR16F1, Japan, and JSPS KAKENHI Grant numbers 18H03676.

Author contributions

D.K. constructed the theory, conducted the calculations, analyzed the data, and wrote the paper. N.N. conceived the study, constructed the theory, and wrote the paper.

Competing interests

The authors declare no competing interests.

Additional information

Supplementary information The online version contains supplementary material available at <https://doi.org/10.1038/s42005-021-00765-3>.

Correspondence and requests for materials should be addressed to Daichi Kurebayashi.

Peer review information *Communications Physics* thanks the anonymous reviewers for their contribution to the peer review of this work.

Reprints and permission information is available at <http://www.nature.com/reprints>

Publisher’s note Springer Nature remains neutral with regard to jurisdictional claims in published maps and institutional affiliations.



Open Access This article is licensed under a Creative Commons Attribution 4.0 International License, which permits use, sharing, adaptation, distribution and reproduction in any medium or format, as long as you give appropriate credit to the original author(s) and the source, provide a link to the Creative Commons license, and indicate if changes were made. The images or other third party material in this article are included in the article’s Creative Commons license, unless indicated otherwise in a credit line to the material. If material is not included in the article’s Creative Commons license and your intended use is not permitted by statutory regulation or exceeds the permitted use, you will need to obtain permission directly from the copyright holder. To view a copy of this license, visit <http://creativecommons.org/licenses/by/4.0/>.

© The Author(s) 2021